HHS Public Access

Author manuscript

Cell Rep. Author manuscript; available in PMC 2025 March 10.

Published in final edited form as:

Cell Rep. 2025 January 28; 44(1): 115148. doi:10.1016/j.celrep.2024.115148.

Acetylation at lysine 27 on maternal H3.3 regulates minor zygotic genome activation

Jiaming Zhang (张加明)[1,2,4,*], **Xuanwen Li (李轩文)**[1,4], **Qi Zhao (赵芪)**[1,4], **Jingzhang Ji (季敬璋)**[1,4], **Hongdi Cui (崔洪帝)**[1], **Weibo Hou (侯卫博)**[1], **Xinyu Wang (王心宇)**[3], **Entong Song (宋恩童)**[1], **Songling Xiao (肖松龄)**[1], **Shukuan Ling (凌树宽)**[1], **Shaorong Gao (高绍荣)**[3,*], **Xiaoyu Liu (刘晓雨)**[3,*], **Duancheng Wen (文端成)**[2,*], **Qingran Kong (孔庆然)**[1,5,*]

[1]Oujiang Laboratory, Zhejiang Provincial Key Laboratory of Medical Genetics, Key Laboratory of Laboratory Medicine, Ministry of Education, School of Laboratory Medicine and Life Sciences, Wenzhou Medical University, Wenzhou, Zhejiang, China

[2]Ronald O. Perelman and Claudia Cohen Center for Reproductive Medicine, Weill Cornell Medicine, New York, NY 10065, USA

[3]Frontier Science Center for Stem Cell Research, School of Life Sciences and Technology, Tongji University, Shanghai 200092, China

[4]These authors contributed equally

[5]Lead contact

SUMMARY

Zygotic genome activation (ZGA) initiates transcription in early embryogenesis and requires extensive chromatin remodeling, including rapid incorporation of the histone variant H3.3. The distinct sources of H3.3 from paternal and maternal alleles (paH3.3 and maH3.3) complicate tracking their individual contributions. Here, using an H3.3B-hemagglutinin (HA)-tagged mouse model, we profile the temporal dynamics of paH3.3 and maH3.3, revealing a unique pattern of maH3.3 enrichment at the promoter regions from zygotes to 2-cell embryos, highlighting the crucial role of maternally stored H3.3 mRNAs and proteins (mH3.3) in pre-implantation development. Knockdown of mH3.3 compromises cleavage and minor ZGA. Mechanistically, mH3.3 facilitates minor ZGA through H3.3S31ph-dependent H3K27ac deposition. Profiling of H3.3 landscape in parthenogenetic (PG) and androgenetic (AG) embryos highlights the role of

*Correspondence: jmzhang1225@163.com (J.Z.), gaoshaorong@tongji.edu.cn (S.G.), liuxiaoyu@tongji.edu.cn (X.L.), duw2001@med.cornell.edu (D.W.), kqr721726@163.com (Q.K.).

AUTHOR CONTRIBUTIONS

D.W., X. Liu, Q.K., and S.G. conceived and designed the study. J.Z. and Q.Z. performed and analyzed most experiments, with significant contributions by H.C., S.X., E.S., and S.L. X. Li, J.J., W.H., and X.W. analyzed chromatin immunoprecipitation sequencing (ChIP-seq), RNA-seq, and ATAC-seq datasets and plotted the bioinformatics figures. J.Z. and H.C. generated most of the sequencing libraries. D.W., X. Liu, Q.K., and S.G. provided critical materials. D.W. and S.G. supervised the study. J.Z., D.W., and Q.K. wrote the manuscript with contributions from all authors. All authors read and approved the final manuscript.

DECLARATION OF INTERESTS

The authors declare no competing interests.

SUPPLEMENTAL INFORMATION

Supplemental information can be found online at https://doi.org/10.1016/j.celrep.2024.115148.

mH3.3 in remodeling the paternal genome by establishing H3K27ac. These findings demonstrate that mH3.3-mediated parental chromatin reprogramming is essential for orchestrating minor ZGA.

In brief

H3.3 is a key maternal factor essential for chromatin remodeling. Zhang et al. generate a parental allele-derived H3.3 genome-wide landscape using a H3.3B-HA mouse model and provide insights into the role of maternal H3.3 in minor zygotic genome activation by establishing acetylation at lysine 27.

Graphical Abstract

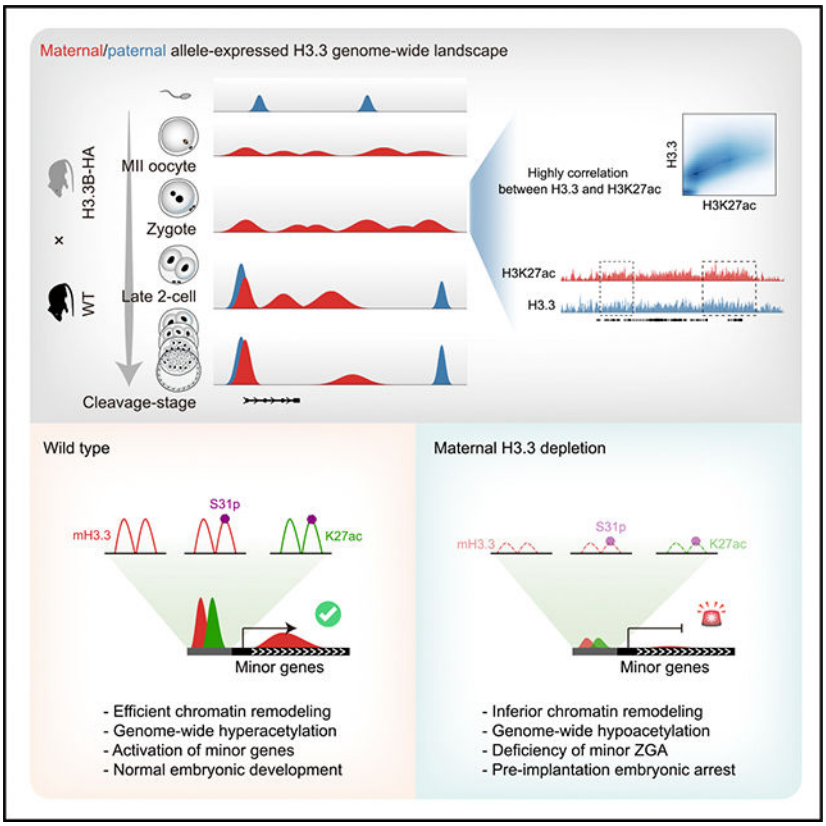

INTRODUCTION

Embryogenesis begins with the fusion of two fully differentiated gametes, egg and sperm, giving rise to a diploid zygote.[1,2] Initially, the development is mainly governed by maternal factors present in the egg's cytoplasm, while the zygotic genome remains inactive.[3,4] As development progresses, both the maternal and paternal genomes undergo extensive chromatin reprogramming to facilitate zygotic genome activation (ZGA), which is characterized by the activation of a group of genes, such as *Dux*.[5,6] In mice, the initial ZGA occurs between the S phase of the zygote and G1 of the early 2-cell embryo, termed minor ZGA, which distinguishes it from the subsequent burst of transcription during the mid-to-late 2-cell stage, known as major ZGA. Minor ZGA precedes major ZGA and is

crucial for the successful execution of the maternal-to-zygotic transition.[7,8] The timely onset of minor ZGA is critical for pre-implantation development to progress beyond the 2-cell stage.[9]

Various aspects of epigenetic reprogramming (herein defined as heritable changes in chromatin structure without altering the nucleotide sequence, such as DNA methylation and histone modifications) are associated with minor ZGA.[10–14] Nucleosome dynamics and properties are central factors in various epigenome regulatory networks, which consist of 147 base pairs of DNA wrapped around histone proteins, containing two sets of H2A, H2B, H3, and H4.[15] With evolution, the number of histone variants has increased. Despite the high similarity in their amino acid sequences, each histone variant can modulate chromatin structure and function in diverse ways, thereby regulating complex biological processes.[16] Histone H3 encompasses more than five different variants, including replicative variants H3.1/H3.2 and a replacement variant H3.3. In mammals, H3.3 is encoded by two different genes (*H3f3a* and *H3f3b*), which give rise to an identical protein product.[17] Its incorporation is mediated by the histone regulator A (HIRA) or death domain-associated protein-alpha thalassemia/mental retardation syndrome, X-linked (DAXX-ATRX) complexes in a cell-cycle-independent manner.[18,19] H3.3 plays a crucial role in the reprogramming of paternal and maternal genomes during fertilization,[20–23] owing to its unique characteristic of being incorporated into chromatin independent of DNA replication. In contrast, its canonical counterparts H3.1 and H3.2 are deposited into chromatin in a DNA replication-dependent manner.[24] This feature distinguishes H3.3 as the sole H3 variant that forms nucleosomes and facilitates genome remodeling prior to the first round of DNA replication before ZGA.

In zygote, H3.3 is composed of paternal allele-derived H3.3 (paH3.3) and maternal allele-derived H3.3 (maH3.3), including maternal stored H3.3 mRNAs and proteins (mH3.3). We previously reported that paH3.3 is rapidly removed from the sperm genome post fertilization, while mH3.3 is integrated into the paternal genome as early as 1 h post fertilization and retained until the morula stage, promoting chromatin decondensation and pronucleus formation, which underscore the critical role of mH3.3 in fertilization and early embryonic development.[21,23] A major challenge arises due to the coexistence of these distinct sources of H3.3 in early embryos. This concurrent presence complicates our ability to precisely track the individual dynamics of H3.3, which may have distinct roles in embryonic development. Consequently, several questions remain unanswered, particularly regarding the specific deposition of mH3.3 and how this deposition contributes to the initiation of ZGA and the reprogramming of the parental genomes.

In this study, leveraging our H3.3B-hemagglutinin (HA)-tagged mouse model, we delineated the paH3.3 and maH3.3 landscapes in mouse early embryos and demonstrate the essential role of mH3.3 in minor ZGA through mH3.3S31phmediated establishment of acetylation at lysine 27. Furthermore, we highlighted the central role of mH3.3 in reprogramming the paternal genome by establishing H3K27ac post fertilization.

RESULTS

The specific enrichment of paH3.3 and maH3.3 in mouse early embryos

To investigate the enrichment patterns of paH3.3 and maH3.3 on genome of mouse pre-implantation embryos, respectively, we collected gametes from wild-type (WT) and H3.3B-HA mice and performed intracytoplasmic sperm injection (ICSI) to generate maternal H3.3 allele-tagged (oocyte$^{H3.3B–HA}$ injected with sperm^{WT}) and paternal H3.3 allele-tagged (oocyte^{WT} injected with sperm$^{H3.3B–HA}$) embryos. We then profiled paH3.3 and maH3.3 landscapes from zygote to blastocyst, using an HA antibody by ultra-low-input micrococcal nuclease-based native chromatin immunoprecipitation (ULI-NChIP) (Figure 1A). For validation, the approach was performed on H3.3B-tagged sperms. The signals detected using 200 sperms showed high correlation and similar pattern to those using bulk sperms (Figure S1A). Therefore, approximately 200 embryos at each stage were used to perform ULI-NChIP. We did not obtain available paH3.3 sequencing library in zygotes despite multiple attempts possibly due to the low expressional level of paternal *H3f3b* allele at this stage. The replicates at each stage exhibited strong correlation (Figure S1B; Table S1). The enrichment patterns of H3.3 in oocytes and sperms were globally distinct, and the canonical maH3.3 and paH3.3 enrichment regions were established and showed high similarity to each other at the 4-cell stage and onwards (Figures 1B, 1C, and S1C). To further support the robustness of our data, we merged our maH3.3 and paH3.3 data at each stage and performed parallel analysis similar to that conducted by the previous study.[20] By calculating the breadth of H3.3 enrichment domains at each stage based on the merged, maH3.3 and paH3.3 data, we clearly showed that the distribution pattern of H3.3 underwent a transition from broad (non-canonical) to sharp (canonical) patterns at the late 2-cell stage (Figure S2A). We observed the enrichments of H3.3 at the transcription start sites (TSSs) inmetaphase II (MII) oocytes, zygotes, and 2-cell embryos, and their deletion happened at the four-cell stage and onwards and progressively accumulated at promoters and gene bodies (Figure S2B). Furthermore, the cluster analysis of the merged maH3.3 and paH3.3 data exhibited highly similar enrichment patterns shown by the previous study (Figure S2C),[20] and we found that gene expression levels positively correlated with H3.3 enrichments at the promoters and gene bodies (cluster I/II) (Figure S2C). For genes in cluster III/IV with the enrichments of H3.3 at the promoters and gene bodies mutually exclusive, particularly at the 2-cell, 4-cell, and 8-cell stages, they prefer to exhibit junior expressional levels, comparing to cluster I/II genes (Figure S2C), supporting the hypothesis that H3.3 plays a complex role in gene regulatory network.

We also found a strong correlation of the maH3.3 enrichment regions with the published H3.3 genome-wide landscapes; however, the high correlation of paH3.3 with the published data was observed at the 4-cell stage onwards (Figure 1D). Definitely, the distribution of maH3.3, but not paH3.3, was more similar to the established H3.3 landscape in 2-cell embryos (Figures S2D). Interestingly, by analysis of maH3.3 and paH3.3 enrichments, we found that maH3.3 showed a widespread distribution throughout the zygotic genome, resembling that in MII oocytes (Figures 1B and 1E). Notably, maH3.3 enrichment regions covered large fractions of the genome in zygotes (Figure S2E), which was also confirmed by

analyzing the H3.3/H3 percentage using H3 ULI-NChIP of mouse pre-implantation embryo (Figure S2F).

Notably, consistent with the genome annotation of H3.3 enrichment regions (Figures 1F and S2G), maH3.3 tends to be enriched at the promoters and gene bodies of the genes in cluster II/IV, whereas paH3.3 shows a preference for enrichment at the promoters at the 2-cell stage in cluster IV (Figure 1E), suggesting the unique paternal-derived H3.3 dynamics during pre-implantation mouse embryonic development. For those genes (cluster VI) specifically expressed at zygote and 2-cell stage, maH3.3, but not paH3.3, showed significant enrichment at the gene regions (Figures 1E and S2C), highlighting the important role of maH3.3 after fertilization. We also characterized the dynamics of H3.3 at accessible regions and found that the H3.3 patterns showed a positive correlation with assay for transposase-accessible chromatin with high-throughput sequencing (ATAC-seq) signals, and particularly maH3.3 patterns exhibited significantly stronger signals at distal accessible regions at the 2-cell stage (Figures S3A and S3B), indicating the potential role of maH3.3 in priming chromatin state during ZGA. Principal-component analysis (PCA) showed that maH3.3 and paH3.3 exhibited highly dynamic changes throughout pre-implantation development. Intriguingly, we found that maH3.3 enrichment could illustrate a clear visualization of the developmental progress of mouse early embryos, but not paH3.3, further highlighting a more important role of maH3.3 during mouse pre-implantation development (Figure 1G). These results demonstrate the unique dynamics of maH3.3 and paH3.3 enrichment during early mouse embryonic development and propose a role of maH3.3 during the early cleavage stage.

Knockdown of mH3.3 leads to 2-cell arrest and failure of minor ZGA

The dynamic change of maH3.3 enrichment to promoter regions from zygotes to 2-cell embryos inspires us to explore the role of mH3.3 in mouse pre-implantation development. We attempted to knockdown mH3.3 by injecting small interfering RNA (siRNA) and morpholino (MO) targeting *h3f3a* and *h3f3b* into MII oocytes followed by ICSI (Figures 2A and S4A). Successful knockdown of mH3.3 was confirmed by immunostaining at the zygote stage (Figure 2B). The knockdown resulted in approximately 15% of zygotes following ICSI exhibiting abnormal paternal pronuclear formation (Figure S4B). To explore the functional role of mH3.3 in ZGA, we carefully monitored pronuclear formation and collected zygotes with two normal nuclei at 10 h post-ICSI for the subsequent experiments. Development was severely compromised in H3.3 siRNA/MO-injected embryos, with most embryos arrested at the 2-cell stage (Figure 2C). Importantly, the developmental defect could be partially rescued by injecting H3.3 protein, strongly suggesting that the 2-cell arrest was due to mH3.3 knockdown (Figure 2C).

We speculate that the 2-cell arrest observed in H3.3 siRNA/MO-injected embryos is due to the failure of ZGA. To investigate this, we performed RNA sequencing (RNA-seq) analysis of control and H3.3 siRNA/MO-injected embryos at the zygote and late 2-cell stage. Unsupervised hierarchical clustering effectively distinguishes between the control and H3.3 siRNA/MO-injected zygotes (Figure S4C). Interestingly, transcriptome analysis revealed that, while the expression levels of major ZGA genes remained largely unchanged in late

2-cell embryos, minor ZGA genes were significantly downregulated in mH3.3-knockdown zygotes. This suggests a critical role of maH3.3 in the regulation of minor ZGA during mouse pre-implantation development (Figures 2D, S4D, and S4E). To address the impact of mH3.3 on minor ZGA, we performed cleavage under targets and tagmentation (CUT&Tag) for H3.3 deposition and found a significant attenuation in H3.3 signal in H3.3 siRNA/MO-injected zygotes after spike-in normalization, confirmed by immunostaining test (Figures 2E, S4F, and S4G). Furthermore, we found that these minor ZGA genes exhibited a marked decrease in H3.3 deposition at their TSSs, while random genes did not show such a change (Figures 2F, S4H, and S4I), suggesting that the activation of these minor ZGA genes may depend on mH3.3 deposition. Taken together, our results demonstrate that mH3.3 is indispensable for cleavage development, potentially by activating minor ZGA.

Maternal H3.3 acetylated at lysine 27 site regulates minor ZGA

It is well-documented that the transition of genes from a silenced state to an active state necessitates substantial epigenetic reprogramming within the promoter regions.[25–28] In this context, modifications to histone H3 are considered to play significant roles, as postulated by the “histone code” hypothesis.[29,30] Following this understanding, we proceeded to examine which histone modifications are influenced by the deposition of mH3.3 on these minor ZGA genes. Accordingly, we conducted an analysis to evaluate the correlations between mH3.3 and H3 modifications at the zygotic stage. Remarkably, the deposition pattern of mH3.3 mirrored that of H3K27ac, exhibiting similar distribution profiles and displaying a robust correlation with this modification ($r = 0.78$) in zygotes (Figures 3A, 3B, and S5A). Indeed, H3K27ac was prominently enriched at genomic elements that coincided with regions enriched for mH3.3 (Figure 3C).

In line with this, we and others have previously demonstrated the important role of H3K27ac in regulating minor ZGA.[11,13] Thus, we postulated a functional connection between mH3.3, H3K27ac, and minor ZGA. To address this possibility, we first examined H3K27ac signal in mH3.3-knockdown embryos using immunofluorescence staining and found that the enrichment of H3K27ac was remarkably lost (Figure 3D). Furthermore, we also observed substantial reductions in H3K27ac enrichment by CUT&Tag in mH3.3-knockdown embryos, suggesting that the acetylation of mH3.3 at lysine 27 site (mH3.3K27ac) is largely established at the zygote stage (Figure 3E).

We then explore the regulatory role of mH3.3K27ac on gene expression. A total of 10,379 genes, which exhibited loss of mH3.3 enrichment in mH3.3-knockdown embryos were identified. By using a fold change threshold (>1.2) to identify promoters with significant reductions in H3K27ac following mH3.3 removal, 77% of these genes ($n = 8,060$) showed significantly reduced H3K27ac signal, thus termed mH3.3K27ac-associated genes, which covered major of minor genes (Figures 3F and S5B). Notably, among mH3.3K27ac-associated genes, 1,160 exhibited decrease in expressions in mH3.3-knockdown embryos, which constituted 87% (1,160/1,275) of the downregulated minor ZGA genes, termed as mH3.3K27ac-associated minor ZGA genes (Figures 3G and S5C). And, their enrichments of H3K27ac were highly similar with H3.3 patterns in zygotes and were lost when mH3.3 was knocked down, exemplified by *Dux* (Figures S5D and S5E). In summary, our results

demonstrate that mH3.3 regulates minor ZGA genes via the establishment of lysine 27 acetylation at the promoter regions.

Failed mH3.3S31 phosphorylation leads to mH3.3K27ac loss, developmental arrest, and minor ZGA failure

As previous studies demonstrated that the phosphorylation of histone H3.3 at serine 31 influences the acetylation of adjacent lysine residues, which in turn stimulates induced transcription,[31] we wanted to test whether mH3.3S31ph is associated with the establishment of mH3.3K27ac in the mouse zygote. We first examined the phosphorylation status of mH3.3 in the mouse zygote using immunofluorescence staining. As expected, the visible H3.3S31 phosphorylation (H3.3S31ph) signal was detected in the nuclei (Figure 4A). It has been reported that H3.3S31ph could be driven by checkpoint kinase 1 (Chk1).[32] We treated MII oocytes with SB-218078 (the inhibitor of Chk1) and performed ICSI. Treatment with SB-218078 reduced global levels of H3.3S31ph in the nuclei of zygotes and resulted in the reduction of H3K27ac signals (Figures S6A and S6B).

To further test the role of mH3.3 phosphorylation in promoting mH3.3K27ac establishment, we injected WT H3.3 or H3.3S31A (which cannot be phosphorylated) mRNAs into germinal vesicle (GV) oocytes followed by *in vitro* maturation (IVM) and ICSI and determined their effect on mH3.3S31ph and mH3.3K27ac levels (Figure 4B). The injection of H3.3S31A mRNAs had no significant effect on the incorporation of H3.3 into chromatin and IVM (Figures S6C–S6F) but, similar to the phenotype of mH3.3-knockdown zygote development, led to the embryos' failure to develop beyond 2-cell stage (Figures 4C and 4D) and resulted in the reduction of H3S31p and H3K27ac levels compared to the control group (Figures 4E and 4F). CUT&Tag data also confirmed the globally reduced levels of H3K27ac in the H3.3S31A-overexpressed group (Figure S6G). These results reveal the importance of mH3.3S31ph on early embryonic development and mH3.3K27ac establishment. Notably, approximately 63% of the mH3.3K27ac-associated genes showed loss of H3K27ac in the H3.3S31A-overexpressedsa group (Figures 4G, 4H, and S6H). We then investigated whether H3.3S31A-overexpressed embryos displayed defective minor ZGA progression by RNA-seq. Transcriptome analysis revealed the lower expressions of H3.3K27ac-associated minor ZGA genes in the H3.3S31A-overexpressed group (Figures 4I, S6I, and S6J). Overall, these data support a role for mH3.3S31ph-meditated acetylation at lysine 27 in regulation of minor ZGA.

Reprogramming of parental genomes mediated by mH3.3

Given that the significant role of mH3.3 in histone epigenetic reprogramming after fertilization, we sought to examine the precise deposition of mH3.3 on the parental genomes. The correlation analysis showed a high correlation of zygotic H3.3 enrichment with MII oocyte, but not sperm (Figure S7A). The global H3.3 enrichment in the zygote was distinct from that in sperm, suggesting the key role of mH3.3 in extensive reprogramming of the paternal genome.

We profiled the mH3.3 landscape in parthenogenetic (PG) and androgenetic (AG) embryos (two sperms were transferred to enucleated H3.3B-tagged oocytes) at 5 h post-activation

(Figure S7B) and identified the mH3.3-changed regions in PG and AG zygotes, including mH3.3-gain, retain/replace (gametic H3.3 on chromatin to mH3.3), and loss domains, to investigate the function of mH3.3 in parental chromatin reprogramming. Interestingly, although H3.3 patterns of MII oocytes were highly similar to those in zygotes, we also observed the considerable gain and loss of H3.3-enriched regions in PG zygotes. By contrast, most H3.3 enrichment regions in sperm were lost in AG embryos, and over 80% of H3.3-enriched regions were newly obtained (Figures S7C and S7D).

By annotating the changed H3.3 enrichment regions, we found that it mainly occurred in intergenic regions (Figure S7E). Additionally, the dynamic reprogramming led to similar patterns of mH3.3 deposition on maternal and paternal genomes at 5 h post-activation (Figures S7F and S7G). These results indicate the role of mH3.3 in reprogramming of parental genomes after fertilization, especially paternal genome.

Maternal H3.3 reprograms paternal genome to establish H3K27ac

As paternal genome appears to be largely occupied by mH3.3 after fertilization, we then sought to understand how mH3.3 reprograms sperm genome. We profiled mH3.3 patterns in AG embryos at the one-cell (5 h, 12 h after fertilization), 2-cell, 4-cell, and morula stages. We found that sperm H3.3 was replaced by genome-wide non-canonical mH3.3 enrichment regions, particularly from 5 h after fertilization (Figures 5A and S8A). The canonical mH3.3 enrichment regions were established on the paternal genome from the 4-cell stage onward (Figure 5A). PCA showed dynamic changes in mH3.3 enrichment on the paternal genome during the developmental progress of early embryos, highlighting the specific manner of mH3.3 on the reprogramming of the paternal genome at post-5 h, 12 h, and 2-cell stage (Figure 5B).

To investigate the details of mH3.3 dynamics during the reprogramming of the paternal genome, we performed k-means clustering from post-5 h to 2-cell stage and clustered the mH3.3 domains into two major groups (Figure 5C). The mH3.3 signals of cluster I were established from 5 h after fertilization. These domains were enriched in the promoters and was preferentially enriched in the high-CpG promoter regions, consistent with a previous study (Figures S8B and S8C).[33] Most of the covered genes were related to ZGA (Figure S8D). The cluster II H3.3 signals were mainly sperm specific and lost after fertilization (Figure 5C).

Previous studies have shown that the paternal genome exhibited more extensive H3K27ac enrichments than maternal genome in zygotes.[11] We found that the paternal enrichments of H3K27ac exhibited high correlation with patterns of mH3.3 on the paternal genome (Figures 5D, S8E, and S8F). We also identified H3.3-specific regions in AG and PG embryos and examined the corresponding H3K27ac signals at these alleles. Interestingly, both AG- and PG-specific regions displayed higher levels of H3K27ac signals from paternal chromatin (Figure 5E), underscoring the critical role of mH3.3 in the reprogramming of paternal chromatin. Additionally, in line with the enrichment of mH3.3K27ac on minor ZGA genes, we found that mH3.3K27ac on the paternal genome covered 83% (n = 963) H3.3K27acassociated minor ZGA genes (Figure 5F), such as *Dux* (Figure 5G). Altogether,

these data indicate that the paternal genome undergoes substantial reprogramming by mH3.3, which is essential for minor ZGA gene activation.

DISCUSSION

The histone variant H3.3 was initially recognized as a component of active chromatin, with its deposition typically occurring in promoter and enhancer regions associated with active genes.[16] In the study, we delineated the dynamic shifts in maH3.3 and paH3.3 landscapes on the parental genome employing H3.3B-HA reporter mice during early embryonic development. Using functional approaches, we further demonstrate the important role of mH3.3S31ph-mediated acetylation at lysine 27 in minor ZGA, which is indispensable for mouse pre-implantation development.

Early embryonic development is characterized by extensive epigenetic reprogramming, which is involved with dynamic H3.3 incorporation.[34] We previously reported that paH3.3 is rapidly removed from the sperm genome post fertilization, while mH3.3 is integrated into the paternal genome as early as 1 h post fertilization.[21] Thus, it is necessary to investigate the distinct roles of H3.3 from distinct sources in embryonic development. In this study, by using H3.3B-HA reporter mice, we found that maH3.3 and paH3.3 exhibit similar distribution profiles at the 4-cell stage and onwards. Interestingly, the distribution pattern of H3.3 undergoes a transition from broad (non-canonical) to sharp (canonical) patterns at the late 2-cell stage. Previous studies have reported that the inherited or zygotic *de novo* established broad H3 modifications converted into typical sharp peaks at late 2-cell stage, and this is required for the ZGA program. Thus, we suggest that this transition from non-canonical to canonical distributions of H3.3 across the genome may be an underlying factor for the reprogramming of H3 modifications, such as H3K4me3 and H3K27ac, underscoring the importance of H3.3 on the epigenetic reprogramming of the parental genomes post fertilization. It should be noted that we did not observe noticeable H3.3 depletion at the MII oocyte and zygote stages, and the prominent depletion of H3.3 at the TSSs occurs after the onset of major ZGA. This observation is further supported by low-input micrococcal nuclease sequencing (MNase-seq) data from mouse MII oocytes, PN3 zygotes, early two-cell, and late two-cell embryos (data not shown). Therefore, maternal H3.3 within promoters may be primed for epigenetic reprogramming, as partially evidenced by our finding that mH3.3 plays a crucial role in establishing H3K27ac. The comprehensive role of H3.3 in chromatin reprogramming merits further investigation.

Once the sperm enters the egg during fertilization, the paternal DNA must be reorganized to facilitate the transcriptional and regulatory requirements of the early embryo.[2] Using AG embryos, we also propose that mH3.3 has a dual function in the reprogramming of the paternal genome. First, mH3.3 serves as a major H3 variant, participating in the formation of nucleosomes across the paternal genome through a non-canonical pattern during the protamine-to-histone transition prior to DNA replication. Subsequently, mH3.3 is selectively enriched at CpG-rich promoters, which is essential for the activation of minor ZGA genes during early embryogenesis. As expected, the development was highly compromised for mH3.3-knockdown embryos, with embryos arrested at 2-cell stage and impaired minor ZGA genes activation. Thus, developmental deficiency induced by the knockdown of mH3.3

could be attributed to abnormal epigenomic reprogramming. In addition, posttranslational modifications of core histones have been associated with transcriptional regulation in epigenomic reprogramming.[35] Unlike canonical histones, the histone variant H3.3 can be deposited onto chromatin in a replication-independent manner. Therefore, mH3.3 supplied by the oocyte is essential for the reprogramming of the parental genomes before the first round of DNA replication.

Incorporation of H3.3 into chromatin, on gene bodies and promoters, destabilizes the nucleosome structure and facilitates transcriptional activation by generating a more accessible chromatin configuration, especially histone acetylation. Our results reveal that mH3.3 contributes to the regulatory network of minor ZGA via H3.3S31ph-mediated establishment of H3K27ac. H3.3S31ph is detectable and accompanies the incorporation of H3.3 into chromatin after fertilization. Given the high turnover of H3.3, phosphorylation at serine 31 might prime the chromatin structure to recruit acetyltransferases, such as p300/CBP (CREB binding protein), which catalyze the addition of acetyl groups to lysine 27. This is supported by previous studies suggesting that H3.3S31ph could serve as a signal for recruiting specific epigenomic writers responsible for depositing histone modifications.[36] These data suggest that H3.3S31ph may provide preferential access to the transcription machinery.

Histone acetylation promotes open chromatin and gene activation by neutralizing the positive charges on DNA.[37] We and others have showed the important role of H3K27ac in regulating minor ZGA in early embryonic development.[11,13] In the study, we find that mH3.3 showed similar distributions and strong correlation with H3K27ac. H3K27ac signal exhibited substantial reductions in mH3.3-knockdown embryos, showing that the deposition of mH3.3 is essential for H3K27ac establishment. Furthermore, we also found that a failure in mH3.3S31 phosphorylation can lead to a loss of mH3.3K27ac, resulting in minor ZGA failure and developmental arrest. Collectively, our data suggest a critical role of mH3.3S31ph-mediated acetylation at lysine 27 for minor ZGA gene activation, which is vital for early embryonic development.

Limitations of the study

Chromatin immunoprecipitation with next-generation sequencing in population cells generates epigenomic profiles that represent only the population average and genomic tiles. Therefore, we conclude that maH3.3 incorporation contributes to the establishment of H3K27ac at the zygote stage. It seems unable to determine whether H3K27ac modifications occur on the H3.3 tail on the same molecule using current technology. This technical limitation prevents experimental validation of the establishment of maternal H3.3-associated H3K27ac at single-histone resolution.

The main purpose of our study was to profile parental-specific expressed H3.3 genome-wide landscapes. Therefore, both the WT and H3.3B-HA mice used for embryo construction were from the Institute of Cancer Research (ICR) strain. As a result, our data may not allow for the analysis of maternal and paternal genome-specific H3.3 enrichments. In addition, although the distributions of mH3.3 and H3K27ac show high correlation at the zygote stage, we cannot fully conclude that mH3.3 plays exclusive role in establishing

H3K27ac. Alternatively, other H3 variants might be also important for the establishment. It can be proved that approximately 63% of the mH3.3K27ac-associated genes showed loss of H3K27ac in the H3.3S31A-overexpressed group. Therefore, more maternal H3 variants deserve to be explored in future studies.

RESOURCE AVAILABILITY

Lead contact

Further information and requests for resources and reagents should be directed to the lead contact, Qingran Kong (kqr721726@163.com).

Materials availability

All unique reagents generated in this study are available via the lead contact with a completed materials transfer agreement.

Data and code availability

- The sequencing data generated in this study have been deposited in the gene expression omnibus (GEO) repository under the accession number GEO: GSE242960. This paper analyzes existing, publicly available data. The accession numbers for the datasets are listed in the key resources table.
- This paper does not report original code.
- Any additional information required to reanalyze the data reported in this paper is available from the lead contact upon request.

STAR★METHODS

EXPERIMENTAL MODEL AND STUDY PARTICIPANT DETAILS

Animals and oocyte sample collection—Animals were housed and prepared in accordance with the protocol approved by the IACUC of Weill Cornell Medical College (Protocol number: 2014–0061). H3.3B-HA mouse model was generated in our previous study.[44] B6D2F1 and ICR mice were obtained from Taconic Farms (Germantown, NY).

Female mice, aged 6–8 weeks, were superovulated using 5 IU of PMSG (Pregnant mare serum gonadotrophin, Sigma-Aldrich, St. Louis, MO) and 5 IU of hCG (Human chorionic gonadotrophin, Sigma-Aldrich) with a 48-h interval between injections. MII oocytes were collected from superovulated female mice 14–16 h after hCG administration. Embryos were cultured in KSOM medium (MR-121-D; Merck, Kenilworth, NJ, USA) under mineral oil at 37°C in a 5% CO2 incubator.

METHOD DETAILS

Treatment of oocytes with inhibitors—SB-218078 (HY-107407; MedChemExpress, Monmouth Junction, NJ, USA) was dissolved in dimethyl sulfoxide (DMSO). This solution was then diluted to achieve the desired concentration in the maturation medium (SB-218078,

3 μM). Embryos were cultured *in vitro* using KSOM medium with the inhibitor for subsequent analysis. Additionally, 0.05% DMSO served as a negative control.

Plasmid construction—cDNAs encoding mouse *H3f3b* were subcloned into expression plasmids driven by the T7 promoter for *in vitro* transcription of mCherry-tagged sequences. A non-inhibitable *H3f3b* variant was constructed by replacing the S31 residue of human H3f3b with an alanine.

***In vitro* transcription—**To prepare mRNAs for microinjection, we linearized the constructed vectors and purified them using phenol-chloroform, followed by ethanol precipitation. The linearized DNAs were then transcribed *in vitro* with the mMESSAGE mMACHINE Kit (AM1344; Invitrogen, Carlsbad, CA, USA). The transcribed mRNAs were polyadenylated, adding poly(A) tails of 200–250 bp, using the mMACHINE Kit (AM1350; Invitrogen). These mRNAs were then recovered via lithium chloride precipitation and resuspended in nuclease-free water. The resulting synthetic mRNA was frozen and stored at −80°C.

Microinjection—MII oocytes were harvested from superovulated B6D2F1 or ICR females 14–16 h post-hCG injection. The microinjection process utilized a FemtoJet 4i microinjector (Eppendorf, Hamburg, Germany) in tandem with ECLIPSE Ti micromanipulators (Nikon, Tokyo, Japan). Before microinjection, siRNAs and morpholino were pooled to a final concentration of siRNAs at 5 μM and morpholino at 0.5 μM each. We co-injected the mixture of negative siRNA and morpholino with parallel concentration as control group. The mixture was delivered into the oocytes using a piezo-operated microcapillary pipette featuring a 3–5 μm inner diameter. For rescue experiment, 500 ng/μL H3.3 protein (Active Motif, 31295) were co-injected into MII oocytes with the siRNAs-morpholino mixture. After the injection, the oocytes were left to rest at room temperature for 10 min, then shifted to an incubator for another 30 min at a minimum. Subsequently, either ICSI or PG activation was executed. All siRNAs targeting H3f3a/b reported previously,[23] employed in this research and sourced from RiboBio. Morpholino oligos were obtained from GENE TOOLS (Philomath, OR, USA) and designed by followed criterion. Morpholino oligos were designed based on the fact that H3f3a/b is the unique 100% matched the upstream of translated sequence of H3f3a/b, respectively. Moreover, the Tm of candidate morpholino must in the Tm 90°C–110°C range, preferring oligos with Tm over 95C, which means it has quite low predicted RNA affinity for use in mice cells (at ~37°C).

The specific sequences for *H3f3a* and *H3f3b* morpholinos and siRNAs can be found in Table S2. For the overexpression of H3.3S31A in GV oocytes, we collected fully grown GV oocytes from PMSG-primed (44 h) 23-day-old mice. To prevent spontaneous GVBD, these GV oocytes were harvested in M2 medium supplemented with 2 μM milrinone. An amount of approximately 5–10 pL of 250 ng/μL mRNAs was microinjected into the oocyte's ooplasm. These injected oocytes underwent culture in G-1 plus medium containing 2 μM milrinone at 37°C with 5% CO_2 for 6 h to facilitate the translation of the introduced mRNAs. Subsequently, the oocytes were moved to milrinone-free G-1 plus medium. The maturation status (polar body1 extrusion rate) of the MII oocytes was assessed 14–16 h after their release from the milrinone treatment.

Intracytoplasmic sperm injection (ICSI)—For ICSI, a WT sperm head from ICR mice was selected in the PVP droplet using the injection pipette, and each H3.3B-HA oocyte received an injection of one sperm head. To explore the dynamics of histone H3.3 deposition in early mouse embryos, embryos maternally expressing H3.3B-HA (where a WT sperm was introduced into an H3.3B-HA oocyte) and those expressing the paternal allele of H3.3B-HA (in which H3.3B-HA sperm was introduced into a WT oocyte) were harvested separately.

For AG embryos,[21] oocytes were placed in a droplet of HEPES-CZB medium containing 5 μg/mL cytochalasin B, which was prepositioned in the operation chamber on the microscope stage. Utilizing a micromanipulator and a precision glass needle, the spindle-chromosomal complex (SCC) was meticulously extracted from oocytes from H3.3B-HA reporter mice. Two WT sperm heads were introduced into enucleated oocytes sourced. Post-ICSI, embryos were permitted to rest at room temperature for about 10 min before being moved to KSOM medium and incubated at 37°C with 5% (v/v) CO2 in air. For PG embryos, the H3.3B-HA oocytes were activated by being cultured in Ca^{2+}-free CZB medium enriched with 10 mM $SrCl_2$ and 5 μg/mL cytochalasin B for a duration of 5 h. Following this, they were relocated to an incubator and nurtured in advanced KSOM (MR-101-D, Merck) at 37°C with 5% (v/v) CO2 in air.

Immunofluorescence staining—Mouse embryos were fixed in fixative solution (FB002; Invitrogen) for 40 min at room temperature, followed by permeabilization in 1% Triton X-100 (93443, 100 mL; Sigma) for 20 min at room temperature. Embryos were then blocked in blocking solution consisting of 1% bovine serum albumin (BSA) in phosphate-buffered saline (PBS) for 1 h at room temperature after three washes in washing solution (0.1% Tween 20, 0.01% Triton X-100 in PBS). Antibody incubation (Histone H3.3, 91191, Active Motif, Carlsbad, CA, USA; H3.3S31ph, ab92628, Abcam, Cambridge, CB2 0AX, UK; H3K27ac: 39133; Active Motif, Carlsbad, CA, USA) was performed overnight at 4°C. The next day, the embryos were washed in washing solution and incubated with secondary antibodies (Invitrogen) for 1 h at room temperature. After staining with Hoechst, the embryos were washed in washing solution. Embryo imaging was performed using an inverted confocal microscope (TCS SP8; Leica, Wetzlar, Germany) and analyzed using LAS X software (Leica).

ULI-NChIP–seq—For ULI-NChIP–seq, we utilized approximately 100 embryos for each reaction, conducting two to three replicates for every stage. All harvested embryos underwent three wash cycles in a 0.5% BSA in PBS solution to mitigate potential contamination. The ULI-NChIP process was executed as described in a previous study.[39] For each immunoprecipitation reaction, we employed one microgram of the HA antibody. Sequence libraries were crafted using the KAPA Hyper Prep Kit, designed for the Illumina platform (kk8504), in adherence to the manufacturer's guidelines. All the libraries were subsequently sequenced on the Illumina platform, following the specified manufacturer's protocols.

CUT&Tag—CUT&Tag was conducted using the Hyperactive *In-Situ* ChIP Library Prep Kit for Illumina (TD903; Vazyme Biotech, Nanjing, China). For mH3.3-knockdown and

H3.3S31A-injected zygotes, both H3.3 and H3K27ac CUT&Tag procedures were executed 10 h post-ICSI. Embryos were treated with 10 μL of pre-washed ConA beads. To this, 50 μL of antibody buffer and 0.5 μg of the primary antibody were added. The solution was then left to incubate overnight at 4°C. After two washes using dig-wash buffer, the embryos were incubated in 100 μL of the same buffer, now containing 1 μL of the secondary antibody, for an hour at room temperature. Following another pair of washes with 800 μL dig-wash buffer, we added 2 μL of pG-Tn5 and 98 μL of dig-300 buffer to the samples and incubated them for an hour at room temperature. This was followed by two more washes with 800 μL of dig-wash buffer. Subsequently, 300 μL of tagmentation buffer was added, and the samples were incubated at 37°C for an hour. To terminate the reaction, we added 10 μL of 0.5 M EDTA, 3 μL of 10% SDS, and 2.5 μL of 20 mg/mL proteinase K. The samples then underwent phenol-chloroform extraction and ethanol precipitation. PCR amplification of the libraries was carried out under these conditions: an initial step at 72°C for 3 min, denaturation at 98°C for 30 s, followed by 20 cycles of 98°C for 10 s, and annealing at 60°C for 30 s. This was concluded with an extension step at 72°C for 1 min before holding the samples at 4°C. The subsequent clean-up post-PCR involved the addition of 1.5× volume of DNA Clean Beads (N411; Vazyme Biotech). Libraries were allowed to interact with the beads for 10 min at room temperature. After a gentle rinse with 80% ethanol, the libraries were eluted in 20 μL of elution buffer. Sequencing of all libraries was performed on the Illumina NovaSeq 6000 platform, adhering to the manufacturer's guidelines.

ULI-NChIP–seq and CUT&Tag data processing—ChIP-seq and CUT&Tag reads were aligned to the mouse genome (mm10) using Bowtie 2 (version 2.2.5) with a default setting after removing adaptor sequences and low-quality reads by fastp (version 0.12.4). Data reproducibility between replicates was assessed by correlation analysis of mapped read counts across the genome. Then, we pooled the biological replicates for each stage and performed downstream analysis. Drosophila genome DNA was used as spike-in in our experiment. When spike-in was included, reads were mapped to the reference genome in which mm10 and Drosophila genome (Drosophila_melanogaster.BDGP6.32.dna.toplevel) are combined. Reads from PCR duplicates were removed using Picard. After confirming reproducibility between replicates, they were merged using Samtools.

The mouse genome (mm10) was divided into 10 kb bins in a sliding window of 5 kb. The number of ChIP and input reads covering each bin was calculated using the BEDtools intersect with option '-c'. To compute normalized enrichment, normalized ChIP read counts were divided by normalized input read counts. Final bam files were converted to bigWig files of read coverages normalized to RPKM using deepTools (version 3.5.1) bamCoverage. Heatmaps were depicted using computeMatrix and plotHeatmap in deepTools (version 3.5.1) for genes.

Genomic regions (10 kb bin) with ≥0.2 normalized H3.3 enrichment were considered as H3.3-enriched regions. Genomic regions (10 kb bin) with ≥0.1 normalized H3 enrichment were considered as H3-enriched regions. The WashU epigenome browser (http://epigenomegateway.wustl.edu/browser/) was used to visualize ChIP-seq and CUT&Tag data.

Identification of dynamic H3.3 domains—To investigate the changes in H3.3 distributions, we divided the mouse mm10 genome into 1 kb bins and calculated the $\log_2$ ChIP/input values for each bin. The characterization of H3.3 distributions during each timepoint was determined based on the value in each bin was positive or negative. The dynamic H3.3 was judged by the changes in signals of bins among groups.

Histone modification analysis—H3K27ac (GSE185653),[13] Allelic H3K27ac (GSE207222),[11] H3K36me3 (GSE112834),[38] H3K4me3 and H3K27me3 (GSE73952),[39] H3K9me3 (GSE98149)[40] and H3-sperm (GSE79227)[41] ChIP-seq datasets were downloaded from previous publications. ChIP-seq reads were aligned to the mouse genome (mm10) using Bowtie 2 after removing adaptor sequences and low-quality reads using Fastp. Duplicate and low-mapping-quality (MAPQ <5) reads were removed. Heatmaps were generated using deepTools. Final bam files were converted to bigWig files of read coverages normalized to RPKM using deepTools (version 3.5.1) bamCoverage. Heatmaps were depicted using computeMatrix and plotHeatmap in deepTools (version 3.5.1) for autosomal gene. CG site (observed versus expected) was calculated for ±2.5 kb from TSSs.

Identification of aberrant and ZGA gene associated H3K27ac domains—For the zygote stages, we quantified the expression levels for each putative H3K27ac domain using the deeptools tool and compared H3K27ac levels between the control and experimental groups using the DESeq2 package in R. We identified H3K27ac-enriched regions by Macs2 callpeaks with the option '-p 0.05 –nomodel'. And the aberrant H3K27ac domains of the stage were identified using stringent criteria: sum of the normalized H3K27ac levels of the control and treated groups ≥ 1.2 in H3K27ac-enriched regions.

The predefined ZGA genes list was from the previous study.[43] Promoters of the ZGA genes (defined as 3 kb around the transcription start site) that overlapped with the aberrant H3K27ac domains according to the BEDTools intersect tool were defined as ZGA gene H3K27ac domains. Changes in CUT&Tag data were processed and visualized using the computeMatrix and plotHeatmap functions of deepTools. Data were imported using the default settings and all values were normalized to RPKM values and scaled as described above. The retained regions were merged using the merge function in BEDTools v2.30.0 if they were consecutive or overlapped.

RNA-seq—RNA-seq libraries were prepared as previously described.[13] For mH3.3-knockdown and H3.3S31A-injected embryos, RNA-seq were performed at 10 h post-ICSI. Briefly, three embryos were used per reaction, and two replicates were performed for each group. All embryos were washed three times in 0.5% BSA-PBS solution to avoid possible contamination. cDNA was amplified using the single cell full length mRNA-amplification kit (N712, Vazyme). Library preparation was performed using the TruePrep DNA Library Prep Kit (TD501, Vazyme) according to the manufacturer's instructions. Briefly, 50 ng amplification DNA sample was transposed by adding mixture (1×TTBL, 5 μL TTE Mix V50 and H2O) to a final volume of 50 μL and incubated at 55°C for 10 min. The mixture was then purified with 1× DNA Clean Beads (Vazyme, N411). Libraries amplifications were constructed in 50 μL PCR reaction (10 μL 5 × TAB, 5 μL PPM, 5 μL N5 adaptor, 5 μL N7 adaptor and 1 μL TAE) and incubation at 72°C for 3 min and 98°C for 45 s, followed by 6

cycles of amplification (98°C for 15 s, 60°C for 30 s, 72°C for 3 min), and then 72°C for 5 min. Size selection was performed with DNA Clean Beads (Vazyme, N411). All libraries were sequenced using the NovaSeq 6000 (Illumina, San Diego, CA, USA) according to the manufacturer's instructions.

RNA-seq data processing—For RNA-seq analysis of early embryos, FastQC was performed for Illumina reads. We used the Trim Galore software to discard low-quality reads, trim adaptor sequences, and eliminate poor-quality bases. Then, we downloaded the mouse reference genome (genome assembly: mm10) from the Ensembl database and used the HISAT2 software for read alignment. The gene-level quantification approach was used to aggregate raw counts of mapped reads using the featureCounts tool. The expression level of each gene was quantified in terms of the normalized fragments per kilobase of transcript per million mapped reads (FPKM). Next, we used the R package DESeq2 for differential gene expression analysis. KEGG analysis of screened DEGs was performed using the KOBAS online tool (http://kobas.cbi.pku.edu.cn/kobas3/). ZGA genes with credible expression levels, specifically minor ZGA genes at the zygote stage (FPKM >1) and major ZGA genes at the late two-cell stage (FPKM >2), based on our RNA-seq data, were selected for further analysis.

QUANTIFICATION AND STATISTICAL ANALYSIS

Statistical analyses—All statistical analyses were performed using R v4.1.0 software (R Development Core Team, Vienna, Austria). Data are expressed as means ± standard error of the mean (SEM). Differences between means were evaluated using the two-tailed Student's t-test or Wilcoxon rank-sum test. Asterisks indicate significant differences as follows: $*p < 0.05$, $**p < 0.01$, and $***p < 0.001$.

Supplementary Material

Refer to Web version on PubMed Central for supplementary material.

ACKNOWLEDGMENTS

This research was supported by the Zhejiang Province Natural Science Foundation of China (grant no. LY22C120001 to Q.K. and no. LQ24C120002 to J.Z.) and the National Natural Science Foundation of China (no. 32370862 to Q.K.). D.W. was supported by the NIH grants (GM129380 and 1R21OD031973) and the New York State Stem Cell Science Program (NYSTEM; contract C32581GG).

REFERENCES

1. Wilkinson AL, Zorzan I, and Rugg-Gunn PJ (2023). Epigenetic regulation of early human embryo development. Cell Stem Cell 30, 1569–1584. 10.1016/j.stem.2023.09.010. [PubMed: 37858333]
2. Clift D, and Schuh M (2013). Restarting life: fertilization and the transition from meiosis to mitosis. Nat. Rev. Mol. Cell Biol. 14, 549–562. 10.1038/nrm3643. [PubMed: 23942453]
3. Lu X, Gao Z, Qin D, and Li L (2017). A Maternal Functional Module in the Mammalian Oocyte-To-Embryo Transition. Trends Mol. Med. 23, 1014–1023. 10.1016/j.molmed.2017.09.004. [PubMed: 28993030]
4. Jukam D, Shariati SAM, and Skotheim JM (2017). Zygotic Genome Activation in Vertebrates. Dev. Cell 42, 316–332. 10.1016/j.devcel.2017.07.026. [PubMed: 28829942]

5. Eckersley-Maslin MA, Alda-Catalinas C, and Reik W (2018). Dynamics of the epigenetic landscape during the maternal-to-zygotic transition. Nat. Rev. Mol. Cell Biol. 19, 436–450. 10.1038/s41580-018-0008-z. [PubMed: 29686419]
6. Hendrickson PG, Dorá is JA, Grow EJ, Whiddon JL, Lim JW, Wike CL, Weaver BD, Pflueger C, Emery BR, Wilcox AL, et al. (2017). Conserved roles of mouse DUX and human DUX4 in activating cleavage-stage genes and MERVL/HERVL retrotransposons. Nat. Genet. 49, 925–934. 10.1038/ng.3844. [PubMed: 28459457]
7. Schulz KN, and Harrison MM (2019). Mechanisms regulating zygotic genome activation. Nat. Rev. Genet. 20, 221–234. 10.1038/s41576-018-0087-x. [PubMed: 30573849]
8. Schultz RM (2002). The molecular foundations of the maternal to zygotic transition in the preimplantation embryo. Hum. Reprod. Update 8, 323–331. [PubMed: 12206467]
9. Abe KI, Funaya S, Tsukioka D, Kawamura M, Suzuki Y, Suzuki MG, Schultz RM, and Aoki F (2018). Minor zygotic gene activation is essential for mouse preimplantation development. Proc. Natl. Acad. Sci. USA 115, E6780–E6788. 10.1073/pnas.1804309115. [PubMed: 29967139]
10. Ladstätter S, and Tachibana K (2019). Genomic insights into chromatin reprogramming to totipotency in embryos. J. Cell Biol. 218, 70–82. 10.1083/jcb.201807044. [PubMed: 30257850]
11. Wang M, Chen Z, and Zhang Y (2022). CBP/p300 and HDAC activities regulate H3K27 acetylation dynamics and zygotic genome activation in mouse preimplantation embryos. EMBO J. 41, e112012. 10.15252/embj.2022112012. [PubMed: 36215692]
12. Du Z, Zhang K, and Xie W (2022). Epigenetic Reprogramming in Early Animal Development. Cold Spring Harbor Perspect. Biol. 14, a039677. 10.1101/cshperspect.a039677.
13. Li J, Zhang J, Hou W, Yang X, Liu X, Zhang Y, Gao M, Zong M, Dong Z, Liu Z, et al. (2022). Metabolic control of histone acetylation for precise and timely regulation of minor ZGA in early mammalian embryos. Cell Discov. 8, 96. 10.1038/s41421-022-00440-z. [PubMed: 36167681]
14. Aoshima K, Inoue E, Sawa H, and Okada Y (2015). Paternal H3K4 methylation is required for minor zygotic gene activation and early mouse embryonic development. EMBO Rep. 16, 803–812. 10.15252/embr.201439700. [PubMed: 25925669]
15. Ahmad K, Henikoff S, and Ramachandran S (2022). Managing the Steady State Chromatin Landscape by Nucleosome Dynamics. Annu. Rev. Biochem. 91, 183–195. 10.1146/annurev-biochem-032620-104508. [PubMed: 35303789]
16. Loppin B, and Berger F (2020). Histone Variants: The Nexus of Developmental Decisions and Epigenetic Memory. Annu. Rev. Genet. 54, 121–149. 10.1146/annurev-genet-022620-100039. [PubMed: 32857637]
17. Szenker E, Ray-Gallet D, and Almouzni G (2011). The double face of the histone variant H3.3. Cell Res. 21, 421–434. 10.1038/cr.2011.14. [PubMed: 21263457]
18. Lin CJ, Koh FM, Wong P, Conti M, and Ramalho-Santos M (2014). Hira-mediated H3.3 incorporation is required for DNA replication and ribosomal RNA transcription in the mouse zygote. Dev. Cell 30, 268–279. 10.1016/j.devcel.2014.06.022. [PubMed: 25087892]
19. Voon HPJ, and Wong LH (2016). New players in heterochromatin silencing: histone variant H3.3 and the ATRX/DAXX chaperone. Nucleic Acids Res. 44, 1496–1501. 10.1093/nar/gkw012. [PubMed: 26773061]
20. Ishiuchi T, Abe S, Inoue K, Yeung WKA, Miki Y, Ogura A, and Sasaki H (2021). Reprogramming of the histone H3.3 landscape in the early mouse embryo. Nat. Struct. Mol. Biol. 28, 38–49. 10.1038/s41594-020-00521-1. [PubMed: 33169018]
21. Kong Q, Banaszynski LA, Geng F, Zhang X, Zhang J, Zhang H, O'Neill CL, Yan P, Liu Z, Shido K, et al. (2018). Histone variant H3.3-mediated chromatin remodeling is essential for paternal genome activation in mouse preimplantation embryos. J. Biol. Chem. 293, 3829–3838. 10.1074/jbc.RA117.001150. [PubMed: 29358330]
22. Lin CJ, Conti M, and Ramalho-Santos M (2013). Histone variant H3.3 maintains a decondensed chromatin state essential for mouse preimplantation development. Development 140, 3624–3634. 10.1242/dev.095513. [PubMed: 23903189]
23. Wen D, Banaszynski LA, Liu Y, Geng F, Noh KM, Xiang J, Elemento O, Rosenwaks Z, Allis CD, and Rafii S (2014). Histone variant H3.3 is an essential maternal factor for oocyte reprogramming. Proc. Natl. Acad. Sci. USA 111, 7325–7330. 10.1073/pnas.1406389111. [PubMed: 24799717]

24. Goldberg AD, Banaszynski LA, Noh KM, Lewis PW, Elsaesser SJ, Stadler S, Dewell S, Law M, Guo X, Li X, et al. (2010). Distinct factors control histone variant H3.3 localization at specific genomic regions. Cell 140, 678–691. 10.1016/j.cell.2010.01.003. [PubMed: 20211137]
25. Bird A (2007). Perceptions of epigenetics. Nature 447, 396–398. 10.1038/nature05913. [PubMed: 17522671]
26. Spivakov M, and Fisher AG (2007). Epigenetic signatures of stem-cell identity. Nat. Rev. Genet. 8, 263–271. 10.1038/nrg2046. [PubMed: 17363975]
27. Mikkelsen TS, Ku M, Jaffe DB, Issac B, Lieberman E, Giannoukos G, Alvarez P, Brockman W, Kim TK, Koche RP, et al. (2007). Genome-wide maps of chromatin state in pluripotent and lineage-committed cells. Nature 448, 553–560. 10.1038/nature06008. [PubMed: 17603471]
28. Zaret KS, and Mango SE (2016). Pioneer transcription factors, chromatin dynamics, and cell fate control. Curr. Opin. Genet. Dev. 37, 76–81. 10.1016/j.gde.2015.12.003. [PubMed: 26826681]
29. Strahl BD, and Allis CD (2000). The language of covalent histone modifications. Nature 403, 41–45. 10.1038/47412. [PubMed: 10638745]
30. Jenuwein T, and Allis CD (2001). Translating the histone code. Science293, 1074–1080. 10.1126/science.1063127.
31. Martire S, Gogate AA, Whitmill A, Tafessu A, Nguyen J, Teng YC, Tastemel M, and Banaszynski LA (2019). Phosphorylation of histone H3.3 at serine 31 promotes p300 activity and enhancer acetylation. Nat. Genet. 51, 941–946. 10.1038/s41588-019-0428-5. [PubMed: 31152160]
32. Chang FTM, Chan FL, R McGhie JD, Udugama M, Mayne L, Collas P, Mann JR, and Wong LH (2015). CHK1-driven histone H3.3 serine 31 phosphorylation is important for chromatin maintenance and cell survival in human ALT cancer cells. Nucleic Acids Res. 43, 2603–2614. 10.1093/nar/gkv104. [PubMed: 25690891]
33. Delbarre E, Jacobsen BM, Reiner AH, Sørensen AL, Küntziger T, and Collas P (2010). Chromatin environment of histone variant H3.3 revealed by quantitative imaging and genome-scale chromatin and DNA immunoprecipitation. Mol. Biol. Cell 21, 1872–1884. 10.1091/mbc.e09-09-0839. [PubMed: 20375147]
34. Xu Q, and Xie W (2018). Epigenome in Early Mammalian Development: Inheritance, Reprogramming and Establishment. Trends Cell Biol. 28, 237–253. 10.1016/j.tcb.2017.10.008. [PubMed: 29217127]
35. Millán-Zambrano G, Burton A, Bannister AJ, and Schneider R (2022). Histone post-translational modifications - cause and consequence of genome function. Nat. Rev. Genet. 23, 563–580. 10.1038/s41576-022-00468-7. [PubMed: 35338361]
36. Armache A, Yang S, Martínez de Paz A, Robbins LE, Durmaz C, Cheong JQ, Ravishankar A, Daman AW, Ahimovic DJ, Klevorn T, et al. (2020). Histone H3.3 phosphorylation amplifies stimulation-induced transcription. Nature 583, 852–857. 10.1038/s41586-020-2533-0. [PubMed: 32699416]
37. Shahbazian MD, and Grunstein M (2007). Functions of site-specific histone acetylation and deacetylation. Annu. Rev. Biochem. 76, 75–100. 10.1146/annurev.biochem.76.052705.162114. [PubMed: 17362198]
38. Xu Q, Xiang Y, Wang Q, Wang L, Brind'Amour J, Bogutz AB, Zhang Y, Zhang B, Yu G, Xia W, et al. (2019). SETD2 regulates the maternal epigenome, genomic imprinting and embryonic development. Nat. Genet. 51, 844–856. 10.1038/s41588-019-0398-7. [PubMed: 31040401]
39. Liu X, Wang C, Liu W, Li J, Li C, Kou X, Chen J, Zhao Y, Gao H, Wang H, et al. (2016). Distinct features of H3K4me3 and H3K27me3 chromatin domains in pre-implantation embryos. Nature 537, 558–562. 10.1038/nature19362. [PubMed: 27626379]
40. Wang C, Liu X, Gao Y, Yang L, Li C, Liu W, Chen C, Kou X, Zhao Y, Chen J, et al. (2018). Reprogramming of H3K9me3-dependent heterochromatin during mammalian embryo development. Nat. Cell Biol. 20, 620–631. 10.1038/s41556-018-0093-4. [PubMed: 29686265]
41. Jung YH, Sauria MEG, Lyu X, Cheema MS, Ausio J, Taylor J, and Corces VG (2017). Chromatin States in Mouse Sperm Correlate with Embryonic and Adult Regulatory Landscapes. Cell Rep. 18, 1366–1382. 10.1016/j.celrep.2017.01.034. [PubMed: 28178516]

42. Wu J, Huang B, Chen H, Yin Q, Liu Y, Xiang Y, Zhang B, Liu B, Wang Q, Xia W, et al. (2016). The landscape of accessible chromatin in mammalian preimplantation embryos. Nature 534, 652–657. 10.1038/nature18606. [PubMed: 27309802]
43. Park SJ, Komata M, Inoue F, Yamada K, Nakai K, Ohsugi M, and Shirahige K (2013). Inferring the choreography of parental genomes during fertilization from ultralarge-scale whole-transcriptome analysis. Genes Dev. 27, 2736–2748. 10.1101/gad.227926.113. [PubMed: 24352427]
44. Wen D, Noh KM, Goldberg AD, Allis CD, Rosenwaks Z, Rafii S, and Banaszynski LA (2014). Genome editing a mouse locus encoding a variant histone, H3.3B, to report on its expression in live animals. Genesis 52, 959–966. 10.1002/dvg.22827. [PubMed: 25262655]
45. Ewels P, Magnusson M, Lundin S, and Käller M (2016). MultiQC: summarize analysis results for multiple tools and samples in a single report. Bioinformatics 32, 3047–3048. 10.1093/bioinformatics/btw354. [PubMed: 27312411]
46. Liao Y, Smyth GK, and Shi W (2014). featureCounts: an efficient general purpose program for assigning sequence reads to genomic features. Bioinformatics 30, 923–930. 10.1093/bioinformatics/btt656. [PubMed: 24227677]
47. Kim D, Paggi JM, Park C, Bennett C, and Salzberg SL (2019). Graph-based genome alignment and genotyping with HISAT2 and HISAT-genotype. Nat. Biotechnol. 37, 907–915. 10.1038/s41587-019-0201-4. [PubMed: 31375807]
48. Langmead B, and Salzberg SL (2012). Fast gapped-read alignment with Bowtie 2. Nat. Methods 9, 357–359. 10.1038/nmeth.1923. [PubMed: 22388286]
49. Zhang Y, Liu T, Meyer CA, Eeckhoute J, Johnson DS, Bernstein BE, Nusbaum C, Myers RM, Brown M, Li W, and Liu XS (2008). Model-based analysis of ChIP-Seq (MACS). Genome Biol. 9, R137. 10.1186/gb-2008-9-9-r137. [PubMed: 18798982]
50. Ramírez F, Ryan DP, Gruning B, Bhardwaj V, Kilpert F, Richter AS, Heyne S, Dundar F, and Manke T (2016). deepTools2: a next generation web server for deep-sequencing data analysis. Nucleic Acids Res. 44, W160–W165. 10.1093/nar/gkw257. [PubMed: 27079975]
51. Li H, Handsaker B, Wysoker A, Fennell T, Ruan J, Homer N, Marth G, Abecasis G, and Durbin R; 1000 Genome Project Data Processing Subgroup (2009). The Sequence Alignment/Map format and SAMtools. Bioinformatics 25, 2078–2079. 10.1093/bioinformatics/btp352. [PubMed: 19505943]
52. Quinlan AR, and Hall IM (2010). BEDTools: a flexible suite of utilities for comparing genomic features. Bioinformatics 26, 841–842. 10.1093/bioinformatics/btq033. [PubMed: 20110278]
53. Love MI, Huber W, and Anders S (2014). Moderated estimation of fold change and dispersion for RNA-seq data with DESeq2. Genome Biol. 15, 550. 10.1186/s13059-014-0550-8. [PubMed: 25516281]

Highlights

- Establishing the landscapes of parental allele-derived H3.3 in mouse early embryos
- Maternal H3.3 knockdown leads to deficient minor ZGA and pre-implantation development arrest
- Maternal H3.3K27ac is implicated in the regulation of minor ZGA
- Maternal H3.3 reprograms paternal genome by establishment of H3K27ac

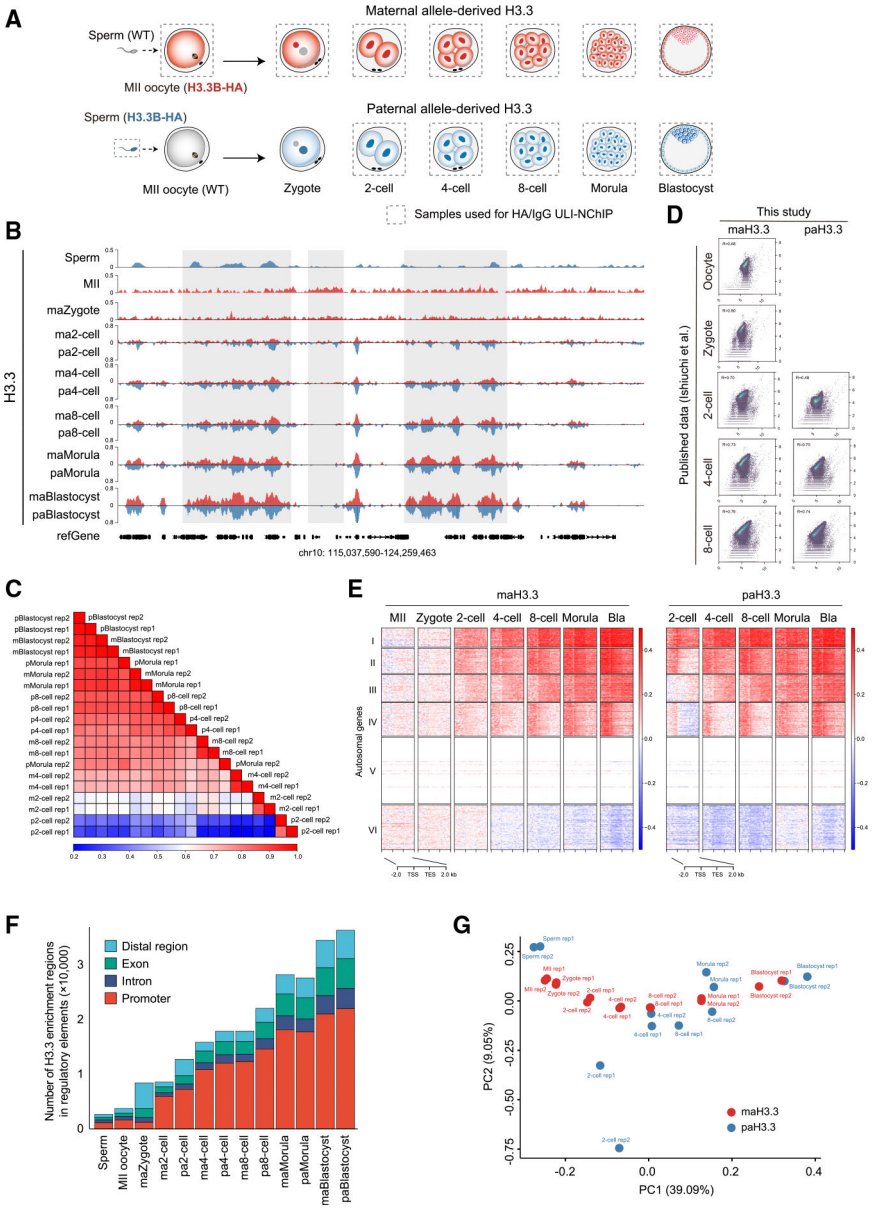

Figure 1. maH3.3 and paH3.3 landscapes in mouse gametes and pre-implantation embryos

(A) Schematic illustration of the experiments. Preimplantation embryos at different stages were collected (>100 embryos each stage) for H3.3B-HA ChIP-seq.

(B) The genome browser view showing enrichment of maH3.3 and paH3.3 signals in mouse gametes and early embryos. Signals represent the $\log_2$-transformed H3.3/input ratio. The maH3.3 and paH3.3 enrichments are indicated in red and blue, respectively.

(C) Correlation heatmaps comparing the maH3.3 and paH3.3 signals between replicates among different developmental stages (two biological replicates).

(D) The Pearson correlation between H3.3 enrichment in this study and a previous study[20] at each stage.

(E) Heatmaps showing maH3.3 and paH3.3 dynamics during mouse pre-implantation development. Bla, blastocyst.

(F) Bar plot showing the H3.3 enrichment regions assigned to the promoter, intron, exon, and intergenic regions. The analyses were performed for 10 kb bins across mouse genome (STAR Methods).

(G) Principal-components analysis (PCA) based on maH3.3 and paH3.3 enrichments in mouse gametes and pre-implantation embryos.

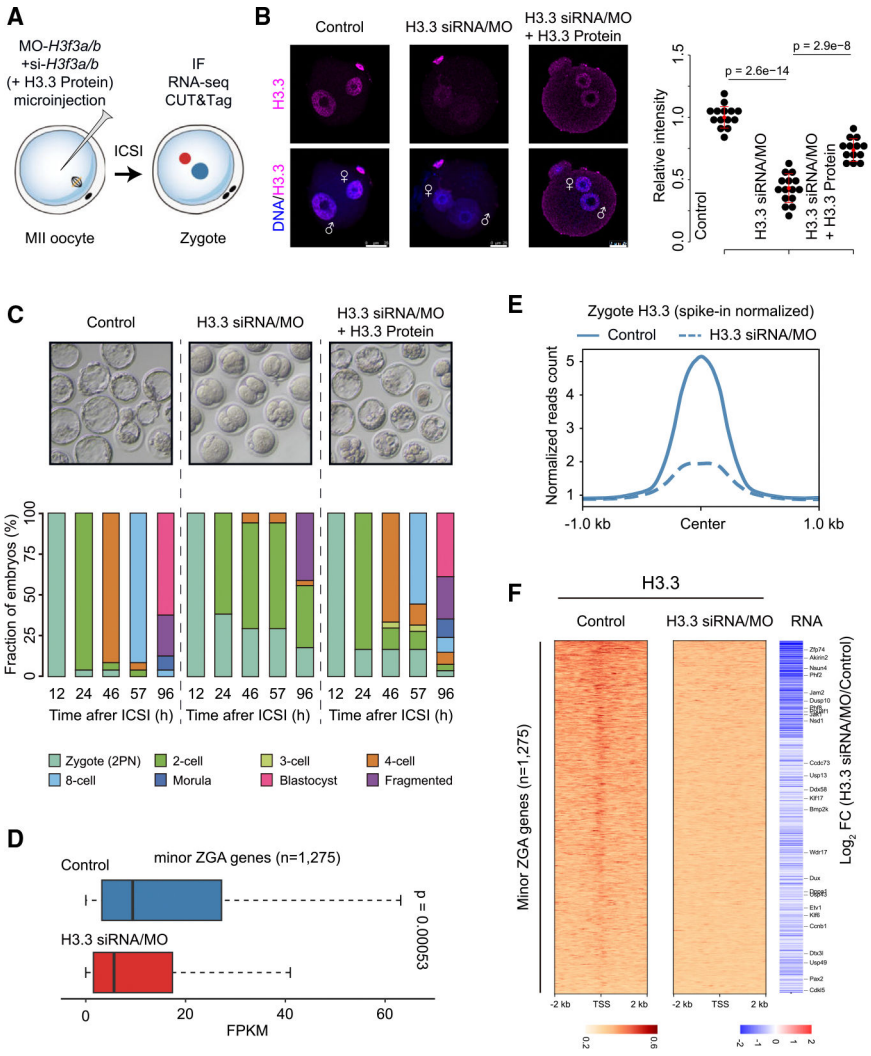

Figure 2. Maternal H3.3 is indispensable for early embryonic development

(A) Schematic presentation of the mH3.3 knockdown experiment protocol.

(B) Left: immunofluorescence of control, H3.3 siRNA/MO, and H3.3 siRNA/MO + H3.3 protein embryos. Scale bar, 25 μm. Right: quantification of H3.3 fluorescence intensity in control, H3.3 siRNA/MO, and H3.3 siRNA/MO + H3.3 protein embryos. Each dot represents a single nucleus. Data are represented as mean ± SEM.

(C) Upper: representative images of the development of control, H3.3 siRNA/MO, and H3.3 siRNA/MO + H3.3 protein embryos. Below: stacked bar plots showing percentage of embryos by stages of development in control (n = 60), H3.3 siRNA/MO (n = 94), and H3.3 siRNA/MO + H3.3 protein (n = 114).

(D) Boxplot showing the minor ZGA genes (n = 1,275) were significantly downregulated in H3.3 siRNA/MO-injected embryos. Data are represented as mean ± SEM.

(E) Metaplot of all H3.3 enrichment regions (spike-in normalized, Z score normalized) in control and H3.3 siRNA/MO-injected zygotes.

(F) Heatmap (left) showing H3.3 signals ranked by their relative changes by mH3.3 knockdown. Heatmap (right) showing the downregulation of minor ZGA genes in H3.3

siRNA/MO-injected embryos. Mean values of two biological replicates were scaled and are represented as Z scores.

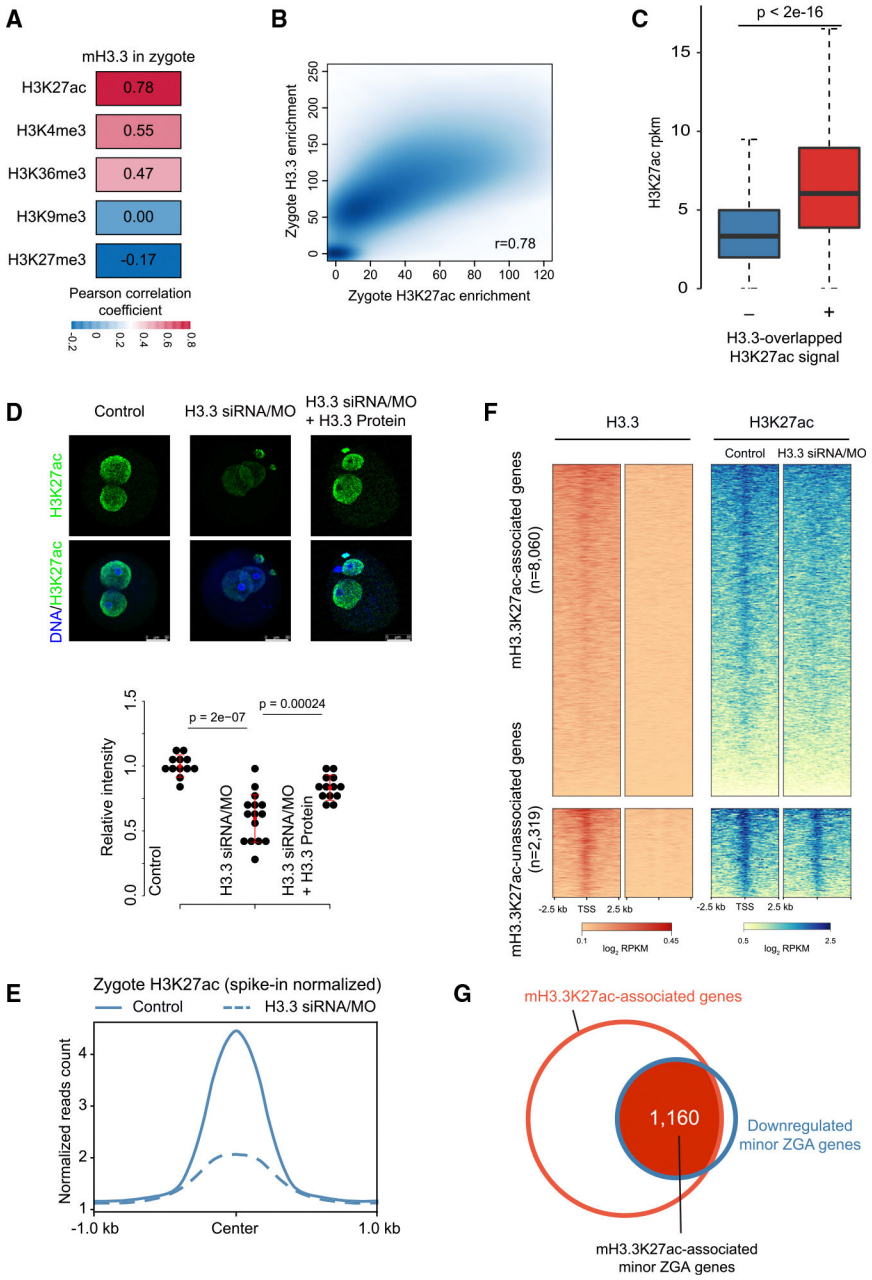

Figure 3. Maternal H3.3 acetylated at lysine 27 site regulates minor ZGA

(A) Global Spearman correlation of H3.3 with other epigenetic markers at zygote stage. Bin size: 1 kb.

(B) Scatterplots showing the comparison of enrichment patterns between H3.3 and H3K27ac at zygote stage. Bin size, 1 kb.</p/>(C) Boxplots showing the comparison of H3K27acrpkm at H3.3- and non-H3.3-enriched regions. Data are represented as mean ± SEM. rpkm, reads per kilobase per million mapped reads.

(D) Upper: representative confocal images of control, H3.3 siRNA/MO, and H3.3 siRNA/MO + H3.3 protein embryos stained with H3K27ac anti-body. Scale bar, 50 μm. Below: quantification of H3K27ac fluorescence intensity in control, H3.3 siRNA/MO, and

H3.3 siRNA/MO + H3.3 protein embryos. Each dot represents a single nucleus. Data are represented as mean ± SEM.

(E) Metaplot of H3K27ac signals (spike-in normalized, Z score normalized) in control and H3.3 siRNA/MO-injected zygotes.

(F) Heatmap analysis of H3.3 and H3K27ac signalsat promoters (n = 10,379) ranked by the change in H3K27ac enrichment after knockdown of mH3.3.

(G) Venn diagrams showing the overlap of mH3.3K27ac-associated genes and down-regulated minor ZGA genes in H3.3 siRNA/MO-injected embryos.

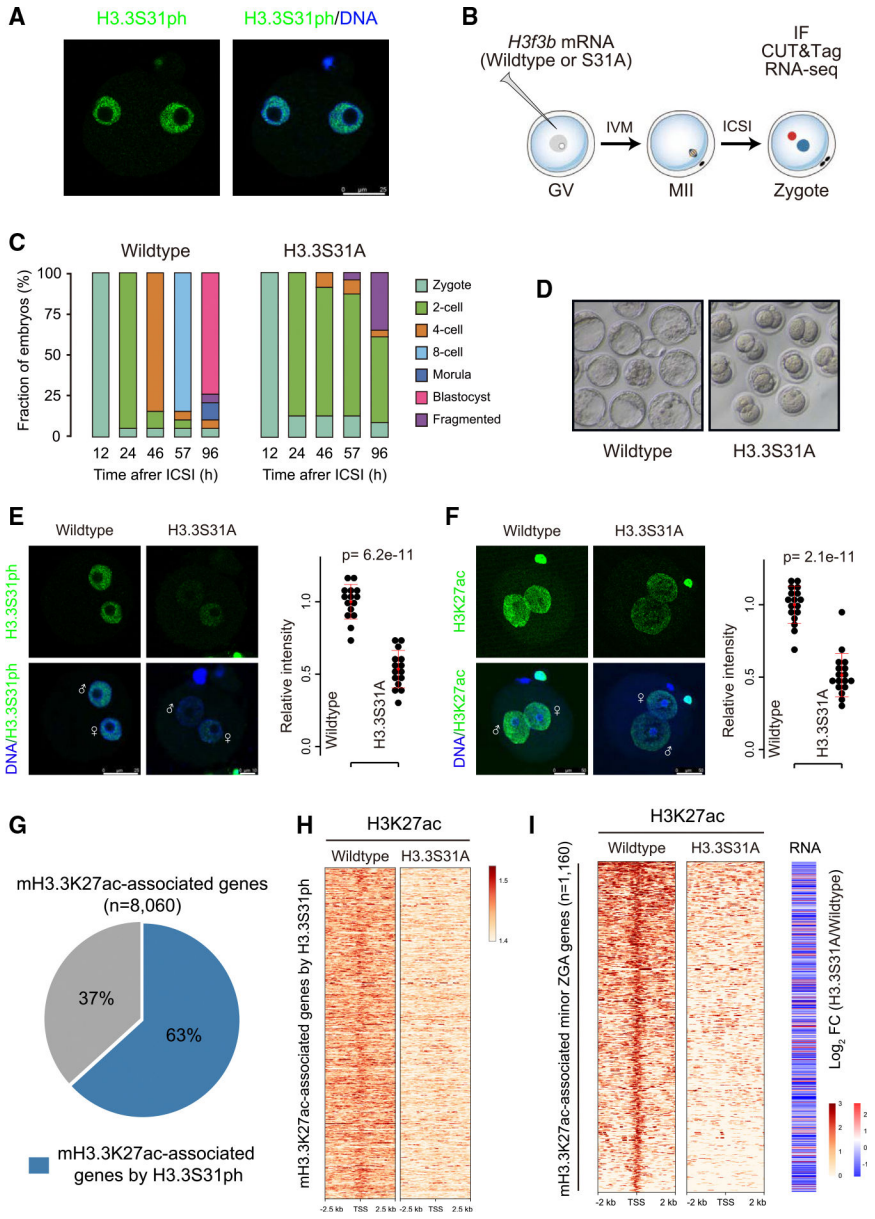

Figure 4. Failed mH3.3S31 phosphorylation leads to mH3.3K27ac loss

(A) Immunostaining for H3.3S31ph in zygotes. Scale bar, 25 μm.

(B) Schematic presentation of the wild-type H3.3 or H3.3S31A injection experimental protocol.

(C) Stacked bar plots showing percentage of embryos by stages of development in the wild-type H3.3-injected (n = 38) and H3.3S31A-injected groups (n = 69).

(D) Representative images of the development of wild-type H3.3 or H3.3S31A-overexpressed mouse embryos.

(E) Left: immunofluorescence of H3.3S31ph.Scale bar, 25 μm or 10 μm. Right: quantification of H3.3S31ph fluorescence intensity in wild-type H3.3 or H3.3S31A-overexpressed zygotes. Each dot represents a single nucleus. Data are represented as mean ± SEM.

(F) Left: immunofluorescence of H3K27ac.Scalebar, 50 μm. Right: quantification of H3K27ac fluorescence intensity in wild-type H3.3 or H3.3S31A-overexpressed zygotes. Each dot represents a single nucleus. Data are represented as mean ± SEM.
(G) Pie chart showing the fraction of mH3.3K27ac-associated genes lost H3K27ac in the H3.3S31A-overexpressed group.
(H) Heatmap showing the loss of H3K27ac signals of mH3.3K27ac-associated genes (n = 5,066) in the H3.3S31A-overexpressed group.
(I) Heatmap (left) showing the loss of H3K27ac signals of mH3.3K27ac-associated minor genes (n = 1,160) in the H3.3S31A-overexpressed group. Heatmap (right) showing the change in expressions of mH3.3K27ac-associated minor ZGA genes (n = 1,160). Mean values of two biological replicates are scaled and represented as Z scores.

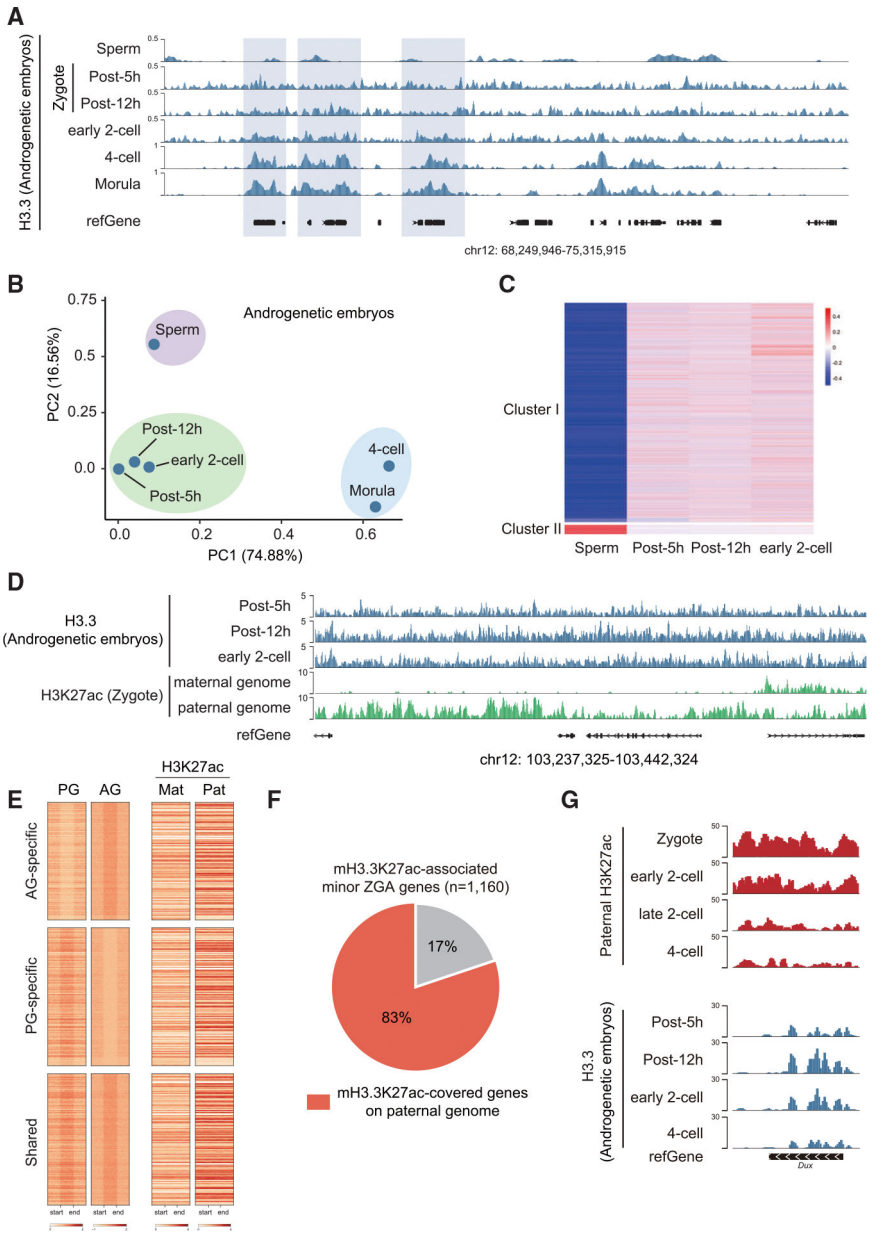

Figure 5. Maternal H3.3 reprograms paternal genome

(A) The genome browser view showing mH3.3 patterns in AG embryos at the zygote, 2-cell, 4-cell, and morula stages.

(B) PCA based on mH3.3 enrichments in AG embryos.

(C) Dynamic changes of mH3.3 patterns in AG embryos. All the mH3.3 domains from sperm to 2-cell were classified into two major clusters using k-means clustering.

(D) The genome browser view shows the paternal enrichments of H3K27ac exhibited high correlation with those of mH3.3 on the paternal genome.

(E) Heatmap showing the AG-specific, PG-specific, and shared H3.3 regions and corresponding H3K27ac signals at maternal and paternal alleles. PG, parthenogenetic embryos; AG, androgenetic embryos; Mat, maternal allele; Pat, paternal allele.

(F) Pie chart showing the fraction of mH3. 3K27ac-associated minor ZGA genes covered by mH3.3K27ac on paternal genome.
(G) Genome browser view of H3.3 and H3K27ac signals on paternal genome at the *Dux* locus.

KEY RESOURCES TABLE

REAGENT or RESOURCE	SOURCE	IDENTIFIER
Antibodies		
Mouse Recombinant anti-H3.3	Active Motif	Cat# 91191; RRID: AB_2793796
Rabbit polyclonal anti-H3	Abcam	Cat# ab1791; RRID: AB_302613
Rabbit Monoclonal anti-H3.3S31ph	Abcam	Cat# ab92628; RRID: AB_10563637
Rabbit Polyclonal anti-H3K27ac	Active Motif	Cat# 39133; RRID: AB_2561016
Rabbit monoclonal anti-HA-Tag	CST	Cat# 3724; RRID: AB_1549585
Chemicals, peptides, and recombinant proteins		
SB-218078	MCE	HY-107407
Recombinant Histone H3.3	Active Motif	Cat# 31295
Micrococcal Nuclease	NEB	M0247S
dsDNA Fragmentase	NEB	M0348S
Poly(ethylene glycol)	Sigma-Aldrich	81255-250G
Triton X-100	Sigma-Aldrich	93443-100ML
TWEEN 20	Sigma-Aldrich	P1379
Phenol:Chloroform:Isoamyl Alcohol	Sigma-Aldrich	P3803-100ML
Glycogen	Sigma-Aldrich	10901393001
Protease Inhibitor Cocktail	Sigma-Aldrich	4693116001
Sodium dodecyl sulfate	Sigma-Aldrich	71736-100ML
Magnesium chloride	Sigma-Aldrich	M1028-10X1ML
PMSF	Sigma-Aldrich	93482-50ML-F
Glycine	Sigma-Aldrich	G7126-10MG
Sodium chloride	Sigma-Aldrich	S6546-1L
PMSG	Sigma-Aldrich	G4527
hCG	Sigma-Aldrich	CG10-1VL
Milrinone	Sigma-Aldrich	475840
CZB Medium	Sigma-Aldrich	MR-019
Cytochalasin B	Sigma-Aldrich	C6762
Strontium chloride	Sigma-Aldrich	439665
Dynabeads Protein A	Thermo Fisher	10001D
Formaldehyde	Thermo Fisher	BP531-500
FastDigest SmiI	Thermo Fisher	FD1244
Fixative Solutions	Thermo Fisher	FB002
EDTA, pH8.0	Beyotime	ST066
1M Tris-HCl, pH8.0	Beyotime	ST787
RIPA	Beyotime	P0013B
NP-40	Beyotime	ST366
3M NaAc	Beyotime	ST351
MaXtract High Density	QIAGEN	129046

REAGENT or RESOURCE	SOURCE	IDENTIFIER
AMPure XP	Beckman	A63881
DTT	Abcam	ab141390
DNA Clean Beads	Vazyme	N411
KSOM	Merck	MR-121-D
M2 medium	Merck	M7167
G-1 plus medium	Vitrolife	Cat#10128
Critical commercial assays		
HiScribe T7 ARCA mRNA Kit	NEB	E2060S
KAPA HyperPrep Kit	Roche	kk8504
KAPA Single-Indexed Adapter Kit	Roche	Kk8700
NGS End Repair/dA-Tailing Module	Yeasen	12608ES96
Single Cell Full Length mRNA-Amplification Kit	Vazyme	N712
Hyperactive Universal CUT&Tag Assay Kit	Vazyme	TD903
TruePrep DNA Library Prep Kit	Vazyme	TD501
Deposited data		
ChIP-seq, CUT&tag and RNA-seq data	This study	GSE242960
H3K27ac ChIP-seq	Li etal.[13]	GSE185653
Allelic H3K27ac ChIP-seq	Wang et al.[11]	GSE207222
H3K36me3	Xu et al.[38]	GSE112834
H3K4me3 and H3K27me3	Liu et al.[39]	GSE73952
H3K9me3	Wang et al.[40]	GSE98149
H3-sperm	Jung et al.[41]	GSE79227
ATAC-seq	Wu et al.[42]	GSE66390
ZGA genes	Park et al.[43]	DRA001066
Experimental models: Organisms/strains		
H3.3B-HA reporter mice	In-house[44]	N/A
ICR mice	Charles River	RRID: IMSR_CRL:022
B6D2F1	The Jackson Laboratory	#100006 - B6D2F1/J
Oligonucleotides		
Morpholinos, siRNAs. See Table S2	This paper	N/A
Recombinant DNA		
pGEMHE-mCherry-H3f3b	This paper	N/A
pGEMHE-mCherry-H3f3b-S31A	This paper	N/A
Software and algorithms		

REAGENT or RESOURCE	SOURCE	IDENTIFIER
FastQC	http://www.bioinformatics.babraham.ac.uk/projects	https://www.bioinformatics.babraham.ac.uk/projects/fastqc/
MultiQC	Ewels et al.[45]	https://multiqc.info/
TrimGalore	http://www.bioinformatics.babraham.ac.uk/projects	http://www.bioinformatics.babraham.ac.uk/projects/trim_galore/
featureCounts	Liao et al.[46]	http://subread.sourceforge.net/
HISAT2	Kim et al.[47]	https://github.com/DaehwanKimLab/hisat2
Bowtie2	Langmead et al.[48]	http://bowtie-bio.sourceforge.net/bowtie2/index.shtml
MACS2	Zhang et al.[49]	https://pypi.org/project/MACS2/
deepTools	Ramirez et al.[50]	https://deeptools.readthedocs.io/en/develop/
SAMtools	Li et al.[51]	http://samtools.sourceforge.net/
BEDTools	Quinlan et al.[52]	https://bedtools.readthedocs.io/en/latest/
DESeq2	Love et al.[53]	https://bioconductor.org/packages/release/bioc/html/DESeq2.html
ggplot2	R	https://ggplot2.tidyverse.org/